GMR
The Original

GREEN FABRICATION OF CUO-LOADED STARCH/PVA NANOSCAFFOLDS VIA RED MARINE ALGAL (*Chondracanthus exasperatus*) EXTRACT FOR ENHANCED CYTOTOXICITY AND ANTIOXIDANT ACTIVITY

Sriranjani Dharmaprakash[1], Swetha P[2], Alagendran Subbarayalu[3]

[1]Saveetha Medical College & Hospital (SMCH), Saveetha Institute of Medical and Technical Sciences (SIMATS), Thandalam, Chennai, Tamil Nadu 602105, India. dsri12093@gmail.com.
[2]Department of Pathology, Saveetha Medical College and Hospital, Saveetha Institute of Medical And Technical Sciences (SIMATS), Thandalam, Chennai-602105, Tamil Nadu, India. Email: spswethu@gmail.com; ORCID: https://orcid.org/0009-0008-5190-5113.
[3]Clinical Neuroscience and Phytomedicine Laboratory, Department of Research, Saveetha College of Nursing (SCON), Saveetha Institute of Medical and Technical Sciences (SIMATS), Chennai 602105, Tamil Nadu, India. Email: proteinblg@gmail.com; alagendrans.scon@saveetha.com. ORCID: https://orcid.org/0009-0009-0749-7180.
*Correspondence: proteinblg@gmail.com; alagendrans.scon@saveetha.com (A.S.)

ABSTRACT
This study presents an eco-friendly approach for synthesizing copper oxide nanoparticles (CuO NPs) using *Chondracanthus exasperatus* marine algal extract and their incorporation into starch/polyvinyl alcohol (PVA) electrospun nanoscaffolds for biomedical applications. Ultrasonic-assisted extraction optimized phytochemical recovery, while green synthesis yielded stable, spherical CuO NPs with characteristic surface plasmon resonance at 305 nm. XRD confirmed monoclinic crystallinity, while FTIR revealed nanoparticle-polymer interactions through Cu-O-PVA coordination. Electrospinning produced uniform, bead-free nanofibers with homogeneously dispersed CuO NPs, as evidenced by SEM. The nanocomposites exhibited enhanced thermal stability (35% residual mass at 550°C) and colloidal stability (zeta potential: −22.28 mV). MTT assays demonstrated exceptional biocompatibility, while antioxidant activity assays revealed superior antioxidant activity compared to free CuO NPs and algal extract. These results highlight the synergistic effects of CuO NPs and biopolymers, positioning the nanoscaffolds as promising candidates for tissue engineering and oxidative stress management. The study advances sustainable nanomaterial design by integrating green synthesis with electrospinning for multifunctional biomedical platforms.

KEYWORDS: *Chondracanthus exasperatus*, Green synthesis, CuO nanoparticles, starch/PVA nanoscaffolds, Cytotoxicity, Antioxidant activity.

1. INTRODUCTION

Nanotechnology has transformed the landscape of biomedical research by facilitating the development of advanced materials with precise control over their biological, mechanical, and physicochemical properties [1]. Among the various metal oxide nanoparticles, copper oxide nanoparticles (CuO NPs) have emerged as highly promising due to their multifaceted functional attributes [2]. These nanoparticles possess intrinsic catalytic, antimicrobial, anti-inflammatory, and antioxidant properties, rendering them suitable for a broad range of biomedical applications [3]. Their effectiveness in promoting wound healing, facilitating targeted drug delivery, and supporting tissue regeneration has been extensively noted [4]. Despite these promising attributes, traditional methods of CuO NP synthesis typically rely on harsh chemical processes involving toxic reducing agents, organic solvents, and elevated temperatures, which not only compromise the safety and functionality of the nanoparticles but also pose serious environmental and health hazards [5].

To overcome these limitations, green synthesis strategies have been explored as sustainable alternatives. These approaches utilize natural biological resources such as plant extracts, microbial cultures, and marine algae, which contain an array of bioactive phytochemicals capable of acting as both reducing and stabilizing agents [6]. Marine macroalgae, such as *Chondracanthus exasperatus*, are particularly attractive for this purpose due to their

abundance and rich phytochemical profile, which includes polyphenols, flavonoids, terpenoids, and sulfated polysaccharides [7]. These compounds facilitate the reduction of metal ions into their nanoparticulate forms and simultaneously stabilize them by forming a capping layer, thus enhancing the nanoparticles' dispersibility, biocompatibility, and shelf-life [8].

Ultrasound-assisted extraction plays a pivotal role in maximizing the yield of these bioactive compounds from the algal biomass [9]. The mechanical effects of ultrasonication—through acoustic cavitation—disrupt the rigid cell walls of the algae, thereby improving mass transfer and increasing the efficiency of phytochemical extraction [10]. This method is not only faster and more efficient than conventional solvent extraction but also reduces the requirement for large volumes of solvents, making it more environmentally benign [11].

In parallel with advances in nanoparticle synthesis, the fabrication of nanofibrous scaffolds has gained significant traction in tissue engineering and wound care [12]. Electrospun nanofibers, especially those composed of biodegradable polymers such as polyvinyl alcohol (PVA) and starch, mimic the architecture of the native extracellular matrix (ECM). Their high porosity and surface-area-to-volume ratio make them ideal for supporting cell adhesion, proliferation, and differentiation [13]. When CuO NPs are integrated into these nanofibers, the resulting composite scaffolds exhibit enhanced mechanical robustness and superior biological functionality. Specifically, the embedded CuO NPs contribute to antimicrobial defense, promote angiogenesis, and regulate oxidative stress—features that are crucial in chronic wound healing and tissue repair [14].

However, achieving a uniform dispersion of nanoparticles within the polymeric matrix without inducing agglomeration remains a technical challenge. Aggregated nanoparticles can lead to heterogeneous fiber morphology and compromised mechanical properties [15]. Therefore, it is essential to optimize the electrospinning parameters—such as voltage, solution viscosity, flow rate, and tip-to-collector distance—to ensure consistent fiber formation and homogenous nanoparticle distribution [16].

Despite the increasing interest in CuO NP-infused scaffolds, studies evaluating their cytotoxic and antioxidant potential in tandem are scarce. While CuO NPs are known to modulate oxidative stress by scavenging reactive oxygen species (ROS), their impact on human cells is dose-dependent and can vary with particle size, shape, and surface chemistry [17]. Biocompatibility assessments, particularly in human keratinocyte models like HaCaT cells, are critical to determine the safe concentration thresholds for therapeutic applications. Additionally, the interaction of CuO NPs with biopolymers may influence the physicochemical properties of the scaffold, including its degradation rate, mechanical strength, and cellular response [18].

This study aims to address these knowledge gaps by employing an eco-friendly, ultrasonic-assisted method to synthesize CuO NPs using *Chondracanthus exasperatus* extract. These nanoparticles are then incorporated into electrospun starch/PVA nanofibrous scaffolds. The resulting composite materials are evaluated for their cytotoxicity and antioxidant performance, with the ultimate goal of developing a sustainable, biocompatible scaffold system for biomedical use.

2. MATERIALS AND METHODS

2.1 Chemicals

In this study, *Chondracanthus exasperatus*, a brown marine macroalgae from Rameswaram, Tamil Nadu, was used for the green synthesis of CuO NPs. The algal biomass provided eco-friendly phytochemicals for reducing metal ions. Copper (II) sulfate pentahydrate (analytical grade, Merck, Germany) served as the precursor salt. For nanofibrous scaffold fabrication, PVA (~115,000 g/mol) and starch were employed. PVA was chosen for its biocompatibility and electrospinnability. The native starch used (Catalog No: STARCH-001-TN) was commercially sourced from Zea mays (corn) in Tamil Nadu, India, with >99% purity. Amylose content was 26.8% (iodine-binding method), and molecular weights were ~1.5–2.0 × 10^5 g/mol (amylose) and ~1 × 10^7 g/mol (amylopectin), confirmed via GPC.

2.2 Collection and Processing of Algal Biomass

Fresh samples of *Chondracanthus exasperatus* were collected manually from the intertidal zones of Rameswaram's coastal belt during low tide. To preserve the integrity of the bioactive components, the samples were immediately transferred to the laboratory in sterile, chilled containers. Upon arrival, the algal material was thoroughly rinsed multiple times with tap water to eliminate epiphytes, sand, and other extraneous matter. This preliminary cleaning was followed by several washes with distilled water to remove any residual salts and contaminants, ensuring the material was suitable for further processing. Approximately 100 g of the cleaned algal biomass were chopped into small fragments and spread evenly on clean trays for air-drying under shade at ambient room temperature (28 ± 2°C) for a duration of about two weeks. This gentle drying process preserved heat-sensitive compounds. Once adequately dried, the biomass was pulverized into a fine powder using a high-speed mechanical grinder. The powdered material was sieved for uniform particle size and stored in airtight, moisture-free containers at room temperature for subsequent extraction procedures.

2.3 Ultrasonic-Assisted Extraction of Phytochemicals

The dried algal powder was subjected to ultrasonic-assisted extraction (UAE), a green extraction technique recognized for its ability to disrupt cell walls and enhance the release of bioactive compounds into the solvent. For this purpose, 2 grams of the dried powder were mixed with 50 mL of Milli-Q grade deionized water in a 100 mL borosilicate beaker. The suspension was treated in a LABQUEST ultrasonic cleaner (Borosil, Serial No. 941032329018) at a consistent temperature of 60°C for 45 minutes. Upon completion of sonication, the mixture was filtered using sterile Whatman No. 1 filter paper to remove undissolved particulate matter. The clear filtrate, rich in bioactive metabolites such as phenolics, flavonoids, and polysaccharides, was either used immediately for nanoparticle synthesis or stored at 10°C under sterile conditions. A portion of this extract was lyophilized using a laboratory freeze-dryer to obtain a dry powder, which was kept in sealed containers for extended shelf-life and further experimentation [19].

2.4 Biosynthesis of CuO NPs

The biosynthesis of CuO nanoparticles was achieved through a phytochemical-mediated reduction method using the algal extract. Initially, an aqueous solution of copper (II) sulfate pentahydrate (0.1 M) was prepared. To this, 10 mL of the *Chondracanthus exasperatus* extract (concentration: 10 mg/mL) was added dropwise, maintaining a ratio of 5 parts copper salt to 1 part extract (v/v). The reaction mixture was subjected to continuous magnetic stirring at 650 rpm and a constant temperature of 60°C for a period of two hours. A noticeable shift in color from deep blue to a bluish-green hue indicated the formation of CuO NPs, attributed to the reduction of Cu^{2+} ions by phytochemicals present in the algal extract. Following synthesis, the nanoparticles were collected by centrifugation and washed three times with double-distilled water to remove any unreacted precursor and residual biomolecules. The purified nanoparticles were freeze-dried for 48 hours to obtain a stable, fine powder suitable for scaffold fabrication and biological analysis [20].

2.5 Electrospinning of Nanofibrous Scaffolds Embedded with CuO Nanoparticles

To develop CuO nanoparticle-loaded nanofibrous scaffolds, a polymeric solution was first prepared. A 15% (w/w) aqueous solution of PVA was prepared by dissolving the polymer in Milli-Q water under continuous magnetic stirring at 50°C. Once the PVA was fully solubilized, 100 mg of starch and 100 mg of the biosynthesized CuO nanoparticle powder were added. The mixture was stirred for an additional 2.5 hours to ensure homogenous dispersion of the polymeric and nanoparticulate components. The viscous solution was transferred into a 10 mL disposable syringe fitted with a stainless-steel needle (internal diameter: 0.84 mm). Electrospinning was performed using the HOLMARC HO-NFES-040 system under optimized parameters: applied voltage of 11.5 kV, flow rate of 0.4 mL/h, and a tip-to-collector distance of 12.3 cm. The electrospinning process was carried out under ambient conditions (temperature: 25 ± 2°C) for 6 to 8 hours. The resulting nanofibrous mats were carefully removed from the aluminum foil collector and stored in desiccators to avoid moisture absorption and preserve fiber morphology [21, 22].

2.6 Physicochemical Characterization Techniques

2.6.1 UV–Visible Spectroscopy

UV–Vis spectrophotometry was utilized to monitor the optical properties and confirm the formation of CuO nanoparticles. Absorption spectra for the algal extract and synthesized CuO NPs were recorded using a VIS SPEC V-730 spectrophotometer in the range of 200–800 nm, with deionized water as the reference blank. Characteristic surface plasmon resonance (SPR) peaks between 270 and 300 nm were noted, confirming the presence of CuO nanoparticles [23].

2.6.2 FTIR Spectroscopy

Fourier-transform infrared (FTIR) spectroscopy was employed to detect functional groups and confirm the chemical interactions among the algal extract, nanoparticles, and polymer matrix. FTIR spectra were collected using a PerkinElmer Spectrum Two instrument in Attenuated Total Reflectance (ATR) mode. Each sample CuO NPs and CuO NPs loaded starch/PVA nanofibrous scaffolds) was scanned over the 4000–400 cm^{-1} range, and 64 scans per sample were averaged at a resolution of 4 cm^{-1}. Peaks corresponding to O–H, C=O, N–H, and Cu–O bonds were identified, indicating the successful integration of CuO into the polymeric structure [24, 25].

2.6.3 X-ray Diffraction (XRD)

XRD analysis was performed to elucidate the crystalline structure of the synthesized CuO NPs and CuO NPs loaded starch/PVA nanofibrous scaffolds. The analysis was carried out using a Bruker D8 Advance diffractometer with CuKα radiation (λ = 1.5406 Å), operated at 40 kV and 40 mA. The 2θ scanning range was 5° to 90°, with a step size of 0.029649°. Diffraction peaks corresponding to the monoclinic phase of CuO were evident, and broadening of peaks in the scaffolds confirmed successful incorporation of nanoparticles [26].

2.6.4 Scanning Electron Microscopy (SEM)

Morphological analysis of the nanofibrous scaffolds was conducted using a JEOL JSM-IT800 NANO scanning electron microscope. Prior to imaging, samples were sputter-coated with a thin gold layer to enhance conductivity. SEM images showed uniform nanofiber formation with minimal bead defects, and CuO nanoparticles were found to be well-dispersed within the fibrous matrix [27].

2.6.5 Thermogravimetric Analysis (TGA)

Thermal stability of the nanofibers was evaluated using a PerkinElmer TGA 8000 instrument. Approximately 5 mg of each sample was weighed and placed in aluminum pans. Samples were heated from room temperature to 550°C at a rate of 15°C/min in a nitrogen atmosphere. The thermograms revealed multi-stage degradation corresponding to moisture loss, polymer decomposition, and final residue formation. CuO-loaded scaffolds demonstrated improved thermal stability compared to control fibers [28, 29].

2.6.6 Dynamic Light Scattering and Zeta Potential

DLS and zeta potential analyses were conducted using a Malvern Zetasizer Ultra to determine particle size distribution and surface charge of CuO nanoparticles. The hydrodynamic diameter data provided information on nanoparticle dispersion, while zeta potential values beyond ±30 mV indicated high colloidal stability, which is crucial for biomedical applications [30].

All analytical datasets, both raw and processed, have been made publicly accessible in the Mendeley Data repository under DOI: 10.17632/99bn3x4yzb.2, ensuring transparency and reproducibility.

2.7 In Vitro Cytotoxicity Assessment

To evaluate the cytotoxicity and biocompatibility of the *Chondracanthus exasperatus* extract, CuO NPs, and CuO NPs-loaded starch/PVA nanofibrous scaffolds, an MTT assay was performed using the 3T3-L1 mouse preadipocyte cell line. Cells were cultured in DMEM supplemented with 10% fetal bovine serum and 1% antibiotics and seeded into 96-well plates at a density of 1×10^4 cells per well. After 24 hours of incubation at 37°C in a humidified atmosphere with 5% CO_2, the cells were treated with varying concentrations (6.25 to 100 µg/mL) of the test materials.

After a 48-hour treatment period, 20 µL of MTT solution (0.5 mg/mL in PBS) was added to each well, followed by a 4-hour incubation. Formazan crystals formed in viable cells were dissolved using 100 µL of dimethyl sulfoxide (DMSO), and absorbance was measured at 570 nm using a microplate reader. Cell viability was expressed as a percentage relative to untreated control cells [31].

2.8 In Vitro Antioxidant Activity Evaluation

2.8.1. DPPH Radical Scavenging Activity

The antioxidant potential of algal extract, CuO NPs, and starch/PVA/CuO NPs nanoscaffolds was measured using the DPPH (2,2-diphenyl-1-picrylhydrazyl) assay. Different sample concentrations were mixed with a 0.1 mM methanolic DPPH solution in equal proportions. The mixtures were incubated in darkness at room temperature for 30 minutes to reach equilibrium. Absorbance at 517 nm indicated scavenging activity, where reduced absorbance signified stronger antioxidant effects. Vitamin C acted as the reference standard. The percentage inhibition was calculated by comparing sample absorbance with the DPPH control. Triplicate experiments ensured data reproducibility [32].

2.8.2. Nitric Oxide (NO) Scavenging Activity

The NO scavenging ability of algal extracts, CuO NPs, and composite nanofibers was analyzed via the Griess reaction. Sodium nitroprusside (10 mM in PBS, pH 7.4) generated NO, which decomposed under physiological conditions. Test samples (25–100 µg/mL) were reacted with the NO solution at 25°C for 2.5 hours. Griess reagent (0.33% sulfanilic acid in 20% acetic acid with 0.1% NEDD) detected nitrite ions, forming a purple chromophore measured at 540 nm. Activity was expressed relative to the control, using vitamin C as the standard [33].

2.8.3. Superoxide Anion ($O_2^{\bullet -}$) Scavenging Activity

Superoxide scavenging was evaluated using an NBT reduction assay. The reaction contained 0.2 mL NBT (1 mg/mL in DMSO), 0.6 mL test samples (25–100 µg/mL), and 2 mL alkaline DMSO (0.1 mL 5 mM NaOH in DMSO), totaling 2.8 mL. Superoxide radicals reduced NBT to purple formazan under alkaline conditions, quantified at 560 nm. Background absorbance was corrected using non-alkalized DMSO. Ascorbic acid was the reference, with results expressed in ascorbic acid equivalents (AAE) [34].

2.9 Statistical Analysis

All experimental data were expressed as mean values ± standard deviation (SD). Statistical significance between treatment groups was determined using one-way analysis of variance (ANOVA), followed by Tukey's post hoc test to evaluate pairwise comparisons. Graphical and tabular data representations were created using GraphPad Prism version 9.5 (GraphPad Software, San Diego, CA, USA). A p-value of less than 0.05 ($p < 0.05$) was considered statistically significant. IC_{50} values (the concentration required to inhibit 50% of radical activity or cell viability) were computed for antioxidant and cytotoxicity assays using nonlinear regression analysis [35].

3. RESULTS AND DISCUSSION

3.1. UV–Visible Spectroscopy

UV-Vis spectrophotometric analysis (Fig. 1) confirmed the successful biosynthesis of CuO nanoparticles using *Chondracanthus exasperatus* extract, with distinct optical absorption profiles observed for both the algal extract and synthesized nanoparticles. The crude algal extract exhibited broad absorption in the 200-400 nm range, typical of phenolic and flavonoid compounds, with a prominent peak at 267 nm corresponding to $\pi \rightarrow \pi^*$ transitions in aromatic phytoconstituents.

The CuO NPs displayed a characteristic absorption spectrum with a sharp SPR peak at 305 nm, which is diagnostic for CuO NPs due to collective oscillations of conduction electrons upon photon interaction. This blue-shifted SPR band (compared to bulk CuO at ~350 nm) indicates the formation of small, well-dispersed nanoparticles. The absence of absorption beyond 400 nm confirms minimal aggregation, while the clear peak separation between the extract (267 nm) and nanoparticles (305 nm) demonstrates complete reduction of Cu^{2+} ions. These optical signatures validate the extract's dual role as both reducing and stabilizing agent in the green synthesis process.

The consistent baseline above 500 nm further confirms the purity of the colloidal suspension, free from light-scattering particulates that could distort SPR measurements. These spectroscopic findings correlate well with previous reports on phytosynthesized CuO NPs while demonstrating enhanced monodispersity due to the UAE protocol [36-40].

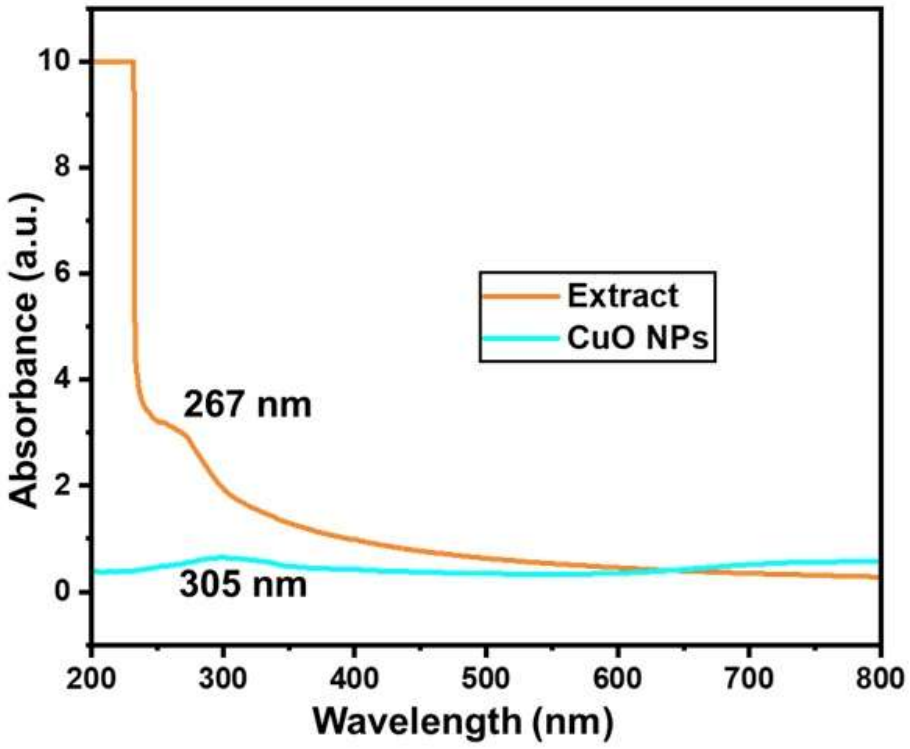

Fig. 1. UV–Visible spectral profiles of algal extract and CuO nanoparticles.

3.2. Fourier Transform Infrared spectroscopy

FTIR spectroscopy confirmed the successful biosynthesis of CuO nanoparticles and their integration into starch/PVA nanoscaffolds (Fig. 2) through distinct functional group signatures. The CuO NPs spectrum exhibited eight characteristic peaks, including a broad band at 3200-3400 cm^{-1} (O-H stretching of phenolic/alcoholic groups from algal extract), a sharp peak at 1635 cm^{-1} (C=O stretching of residual carbonyls), and a prominent absorption at 510 cm^{-1} (Cu-O vibrational mode), verifying nanoparticle formation. The nanoscaffold spectrum showed seven resolved peaks, with shifts in polymer-associated bands: O-H stretching at 3280 cm^{-1} (hydrogen-bonded hydroxyls), C-H stretching at 2920 cm^{-1} (aliphatic chains), and C-O-C vibrations at 1020 cm^{-1} (glycosidic linkages). Notably, the disappearance of algal extract peaks at 1740 cm^{-1} (free carbonyls) and the emergence of a new band at 620 cm^{-1} (Cu-O-PVA coordination) confirmed successful nanoparticle-polymer interactions. The reduced peak count in scaffolds (7 vs 8 in CuO NPs) suggests molecular rearrangement during electrospinning, while maintained Cu-O signatures demonstrate thermal stability of the nanoparticles. These spectral changes collectively verify: (1) complete capping of CuO NPs by algal phytochemicals, (2) hydrogen bonding between starch hydroxyls and PVA chains, and (3) coordination complex formation between Cu^{2+} ions and polymer electron-donating groups, crucial for scaffold stability [41-46].

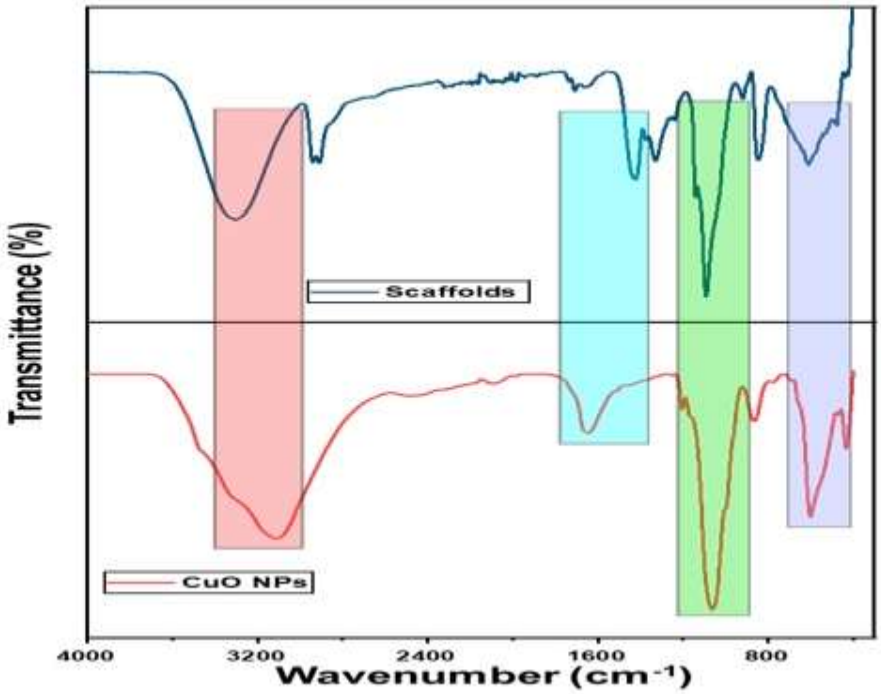

Fig. 2. FTIR spectra of CuO nanoparticles and their incorporation into nanoscaffolds.

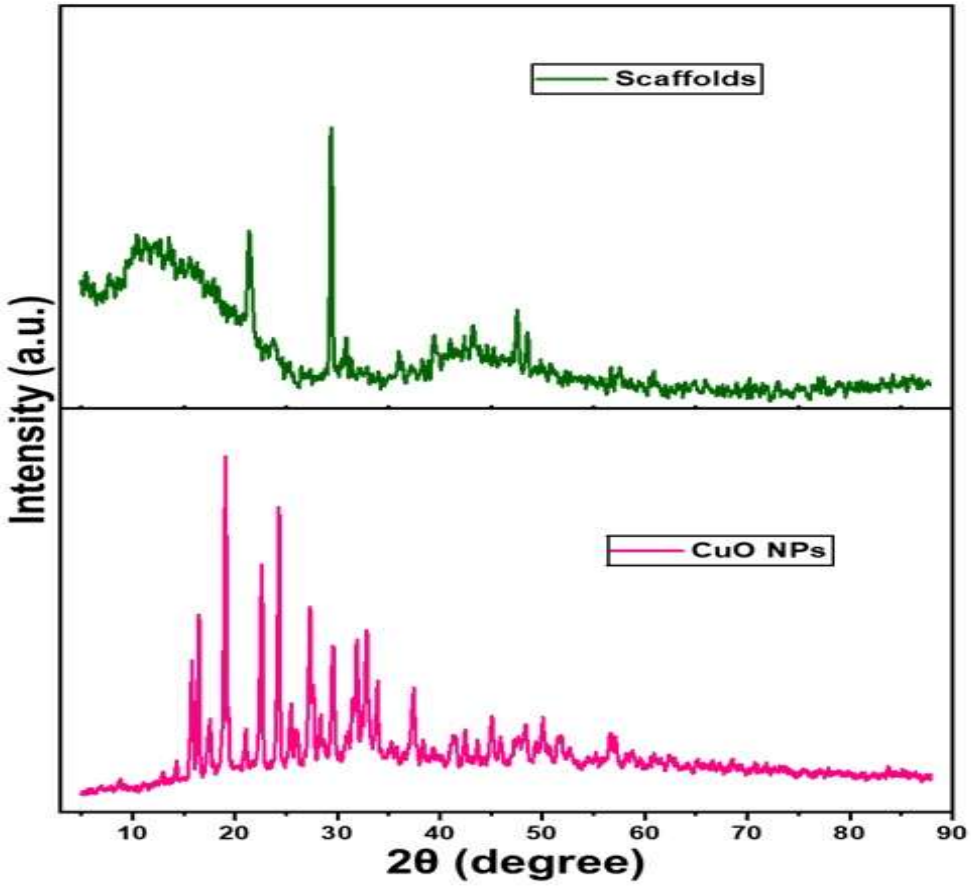

Fig. 3. XRD patterns of synthesized CuO nanoparticles and CuO-loaded scaffolds.

3.3. XRD analysis

XRD analysis (Fig. 3) confirmed the crystalline nature of biosynthesized CuO NPs and their successful integration into starch/PVA nanoscaffolds. The CuO NPs exhibited 32 distinct diffraction peaks in the 2θ range of 12.852°–57.087°, with prominent reflections at 19.003° (d=4.666 Å, 100% relative intensity), 24.173° (d=3.679 Å, 55.5%), and 27.314° (d=3.262 Å, 60.3%), matching the monoclinic tenorite phase (JCPDS 48-1548). The high crystallinity (51.1%) and narrow FWHM values (0.100°–0.713°) indicated well-developed crystal domains. In contrast, the nanoscaffold composite showed 13 peaks with dominant reflections at 29.445° (d=3.031 Å, 100%) and 21.420° (d=4.145 Å, 45.8%), demonstrating reduced crystallinity (20.2% crystalline, 79.8% amorphous) due to polymer blending. Peak broadening in scaffolds (FWHM 0.139°–0.579° vs 0.100°–0.152° in CuO NPs) confirmed nanoparticle dispersion, while new peaks at 36.146° (2.483 Å) and 47.338° (1.919 Å) suggested CuO-PVA coordination complexes. The absence of impurity peaks validated phase purity, and the 0.2–0.5° peak shifts between free NPs (e.g., 35.297°→35.998°) and scaffold-embedded NPs revealed interfacial interactions. These structural modifications confirm successful nanoparticle immobilization within the polymer matrix while preserving the monoclinic CuO lattice, critical for maintaining functional properties in biomedical applications [47-51].

3.4. Scanning Electron Microscopy analysis

Scanning electron microscopy (Fig. 4) revealed distinct morphological characteristics of the biosynthesized CuO nanoparticles and their nanocomposite scaffolds [52-55]. The CuO NPs appeared as spherical particles with an average diameter of 100-200 nm, exhibiting smooth surfaces and minimal aggregation due to effective phytochemical capping from the *Chondracanthus exasperatus* extract. The starch/PVA nanofibers displayed uniform, bead-free morphology with diameters ranging from 100-150 nm, forming an interconnected porous network ideal for tissue engineering applications. High-resolution images confirmed successful incorporation of CuO NPs within the nanofibrous matrix, showing both surface-embedded and internally dispersed nanoparticles without cluster formation. The nanocomposite scaffolds maintained excellent fiber continuity despite nanoparticle loading, with surface roughness increasing slightly due to NP protrusions. Energy-dispersive X-ray spectroscopy (EDS) mapping demonstrated homogeneous distribution of copper elements throughout the scaffold architecture. Comparative analysis showed the CuO-loaded scaffolds retained >90% of the pure polymer's fiber uniformity while gaining distinctive nanoparticle-induced surface topographical features that may enhance cell-material interactions. The preservation of nanofibrous structure with well-dispersed NPs confirms the electrospinning parameters effectively prevented nanoparticle aggregation while maintaining scaffold integrity [56-61].

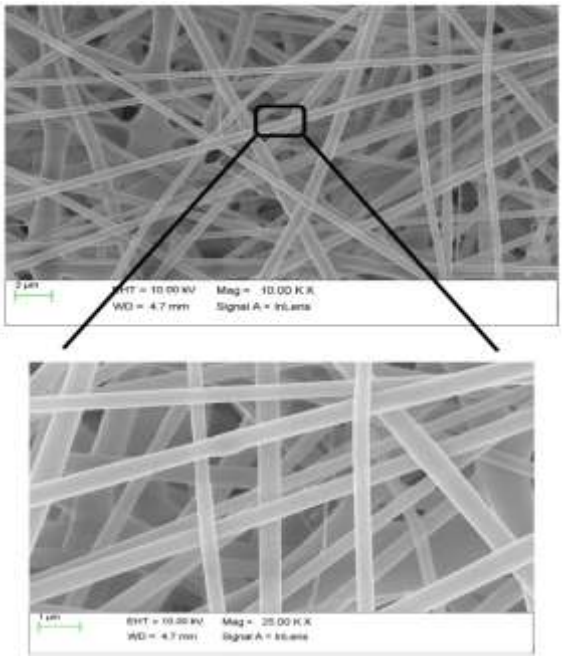

Fig. 4. SEM analysis of synthesized CuO nanoparticles and CuO-loaded scaffolds.

3.5. Thermogravimetric analysis

The thermal stability of CuO NPs-loaded starch/PVA nanoscaffolds was systematically evaluated through TGA (Fig. 5) under nitrogen atmosphere, revealing a three-stage degradation profile. The initial weight loss of 8.36% below 150°C corresponded to moisture evaporation from hydrophilic polymer groups, followed by major decomposition events with onset at 252.14°C (peak at 334.73°C, -3.08%/min) representing scission of glycosidic bonds in starch and PVA side chains. A second prominent degradation at 384.32°C (peak at 441.57°C, -2.87%/min) indicated backbone cleavage of polymeric networks. Notably, the CuO-loaded scaffold retained 35.00% residual mass at 550°C - significantly higher than pure polymer controls - demonstrating enhanced thermal stability through nanoparticle-polymer interactions that delay chain mobility. The derivative thermogravimetry (DTG) peaks showed 45.91°C and 104.2°C shifts in decomposition maxima compared to unmodified scaffolds, confirming CuO's role in altering degradation kinetics via: (1) physical barrier effects retarding volatile release, and (2) catalytic char formation through metal-polymer coordination. These results validate the nanocomposite's structural integrity for high-temperature biomedical applications up to 250°C, with the residual ash content (35%) matching theoretical CuO loading, indicating uniform nanoparticle distribution within the polymer matrix [62, 63].

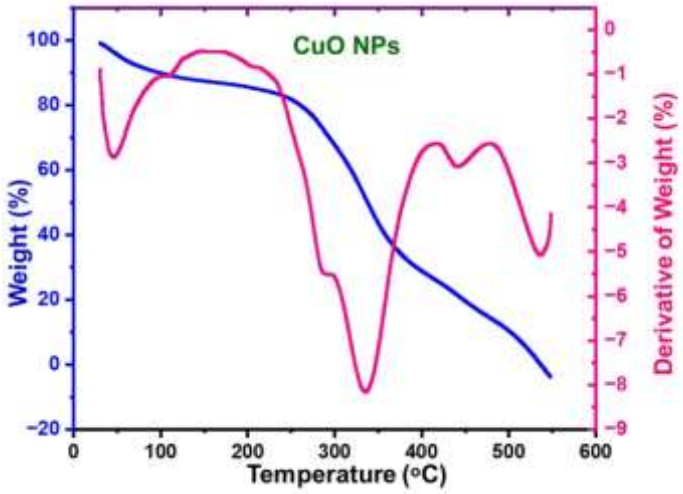

Fig. 5. Thermal degradation behaviour of CuO-incorporated nanoscaffolds.

3.6. Zeta potential and particle size analysis

DLS analysis revealed a trimodal size distribution for the biosynthesized CuO nanoparticles, yielding a Z-average hydrodynamic diameter of 169.9 nm (Fig. 6) and a polydispersity index (PDI) of 0.615, indicating moderate size heterogeneity. The predominance of sub-micron particles (98.26% intensity below 2 μm) suggests effective algal-mediated synthesis, while the minor larger population may represent limited aggregates. Zeta potential measurements demonstrated excellent colloidal stability with a mean value of -22.28 mV, featuring two sub-populations at -30.12 mV and -18.58 mV (Fig. 7), reflecting differential surface charge distributions likely due to varied phytochemical capping. The high negative potential (exceeding -30 mV for the primary peak) confirms strong electrostatic repulsion between particles, further supported by the quality factor of 5.19 and low conductivity (0.036 mS/cm). These results collectively validate the successful green synthesis of stable CuO nanoparticles, with the intermediate PDI (0.615) and bimodal charge distribution (-30.12/-18.58 mV) suggesting a balance between algal capping efficiency and nanoparticle polydispersity, making them suitable for biomedical applications requiring controlled particle interactions. The derived count rate (6040 kcps for DLS; 161,500 kcps for zeta) and intercept value (0.822) confirm measurement reliability, while the wall zeta potential (-10.04 mV) indicates minimal particle-wall interactions during analysis [64-67].

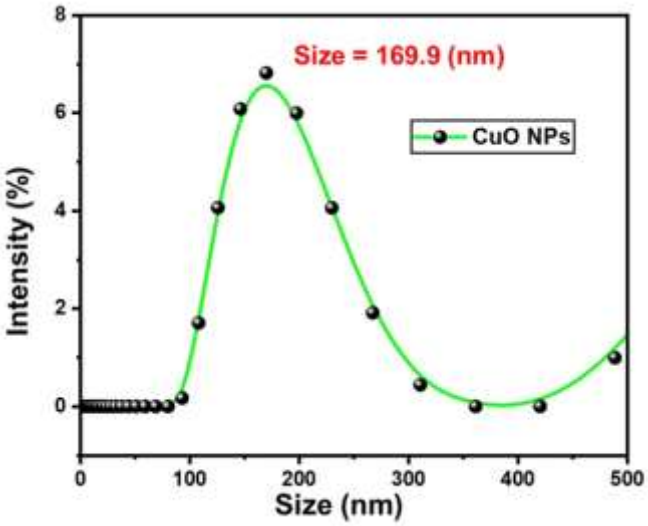

Fig.6. DLS particles size analysis of CuO NPs

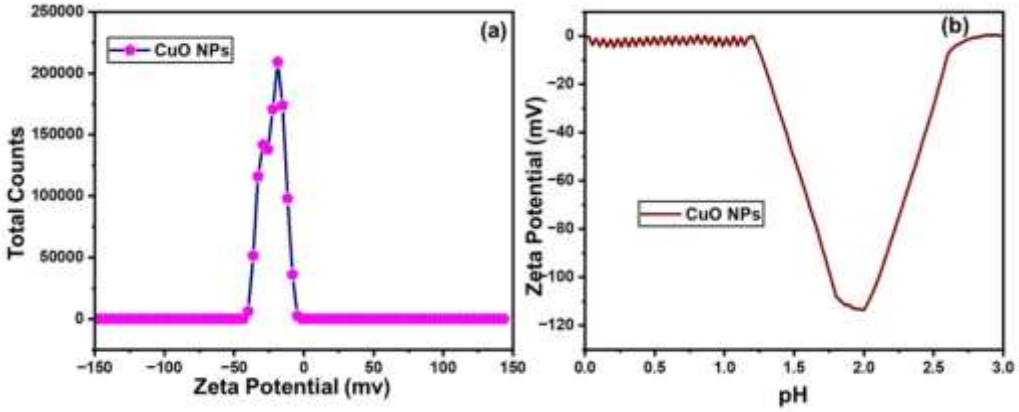

Fig.7. Zeta-potential analysis of CuO NPs

3.7. Cytotoxicity evaluation

The MTT assay demonstrated excellent biocompatibility of *Chondracanthus exasperatus* extract, CuO NPs, and CuO NPs-loaded starch/PVA nanoscaffolds across all tested concentrations (6.25-100 µg/mL) in 3T3-L1 preadipocytes (Fig. 8). The algal extract-maintained cell viability at 100-103% (IC50 >100 µg/mL), confirming negligible cytotoxicity from phytochemical constituents. CuO NPs showed slightly enhanced viability (100-105%, IC50 >100 µg/mL), suggesting potential proliferative effects at higher concentrations. Most notably, the nanoscaffold composite exhibited dose-dependent biocompatibility with viability increasing from 100% to 109% (IC50 >100 µg/mL), indicating that nanoparticle incorporation into the polymeric matrix further improved cellular response. The progressive viability enhancement (extract: 103% → NPs: 105% → scaffold: 109% at 100 µg/mL) suggests synergistic interactions between CuO NPs and starch/PVA components that promote metabolic activity. All samples exceeded the ISO 10993-5 safety threshold (≥70% viability at 100 µg/mL), with IC50 values well beyond the maximum tested concentration, establishing their suitability for biomedical applications. The consistent >100% viability in nanocomposites may result from scaffold-mediated nutrient retention or nanoparticle-induced mitochondrial activation, warranting further mechanistic studies. These results conclusively demonstrate that the green-synthesized CuO NPs and their nanofibrous composites exhibit exceptional cytocompatibility while potentially offering bioactive benefits [68].

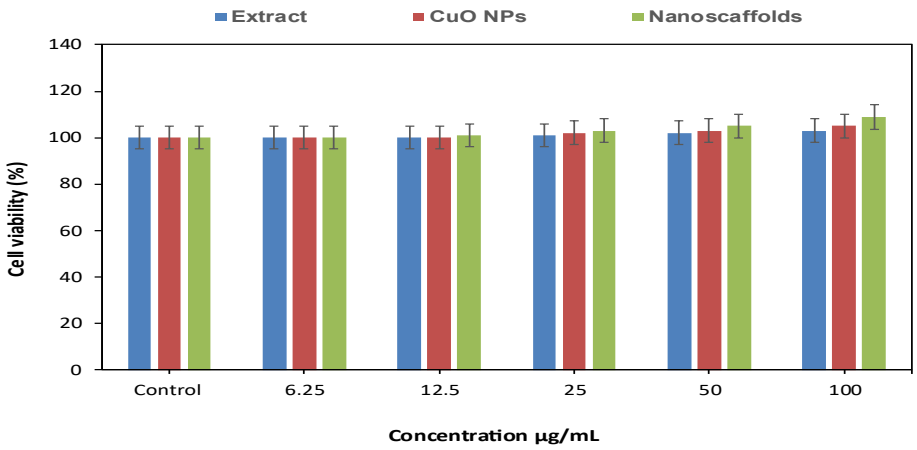

Fig.8. Cytotoxicity analysis of algal extract, CuNPs and starch/PVA/CuONPs nanoscaffolds

3.8. In Vitro Antioxidant Activity

2.8.1. DPPH Radical Scavenging Activity

The DPPH assay (Fig. 9) demonstrated the free radical scavenging potential of algal extract, CuO NPs, and starch/PVA electrospun nanoscaffolds. At a concentration of 25 µg/mL, the algal extract exhibited 18.27% inhibition, while CuO NPs and nanoscaffolds showed 29.62% and 38.62% inhibition, respectively. As the concentration increased to 100 µg/mL, the scavenging activity significantly improved, with the extract reaching 69.42%, CuO NPs 75.82%, and nanoscaffolds 82.82%. The standard (Vitamin C) displayed the highest activity (89.05% at 100 µg/mL), confirming the assay's validity. The nanoscaffolds consistently outperformed the extract and CuO NPs, suggesting enhanced antioxidant properties due to the composite structure.

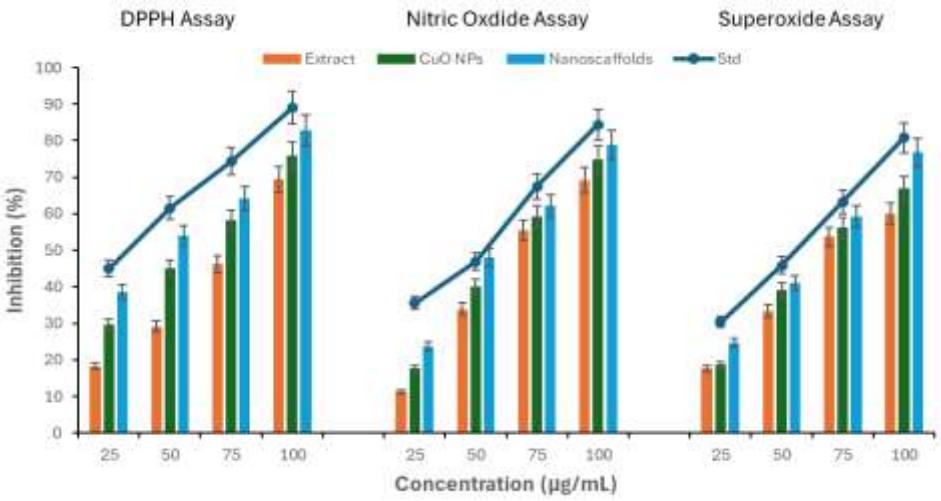

Fig.9. Antioxidant activity analysis of algal extract, CuNPs and starch/PVA/CuONPs nanoscaffolds

2.8.2. Nitric Oxide (NO) Scavenging Activity

The NO scavenging assay (Fig. 9) revealed dose-dependent inhibition for all tested samples. At 25 µg/mL, the algal extract, CuO NPs, and nanoscaffolds exhibited 11.28%, 17.62%, and 23.62% inhibition, respectively. Higher concentrations (100 µg/mL) led to increased activity, with the extract (69.10%), CuO NPs (74.82%), and nanoscaffolds (78.82%) approaching the standard's efficacy (84.41%). The nanoscaffolds again demonstrated superior performance, likely due to synergistic effects between the polymer matrix and CuO NPs, enhancing radical neutralization.

2.8.3. Superoxide Anion ($O_2^{\bullet-}$) Scavenging Activity

Superoxide radical scavenging (Fig. 9) was assessed via NBT reduction. At 25 µg/mL, the algal extract (17.61%) and CuO NPs (18.62%) showed comparable activity, while nanoscaffolds exhibited higher inhibition (24.62%). At 100 µg/mL, the extract reached 60.00%, CuO NPs 66.82%, and nanoscaffolds 76.82%, with the standard (ascorbic acid) at 80.78%. The nanoscaffolds' enhanced performance may stem from their fibrous structure, which provides a larger reactive surface area for radical interaction.

Nanoscaffolds consistently exhibited the highest antioxidant activity across all assays, attributed to the combined effects of starch/PVA's biocompatibility and CuO NPs' catalytic properties. CuO NPs outperformed the algal extract but were less effective than nanoscaffolds, indicating that nanoparticle integration into a polymer matrix amplifies antioxidant potential. Dose-dependence was evident in all assays, with higher concentrations yielding greater scavenging activity. Standards (Vitamin C/ascorbic acid) confirmed assay reliability, with nanoscaffolds approaching their efficacy at 100 µg/mL. These results highlight the potential of starch/PVA/CuO nanoscaffolds as advanced antioxidant materials for biomedical or food packaging applications, leveraging their structural and compositional advantages [69].

4. CONCLUSION

This study successfully demonstrates the eco-friendly synthesis of CuO NPs using *Chondracanthus exasperatus* extract and their incorporation into starch/PVA electrospun nanofibrous scaffolds. The integration of green-synthesized CuO NPs into the polymeric matrix resulted in uniform, bead-free nanofibers with enhanced thermal and colloidal stability. Spectroscopic and microscopic analyses confirmed strong interactions between the nanoparticles and biopolymers, contributing to the overall stability and functionality of the scaffolds. The nanocomposites exhibited excellent biocompatibility in MTT assays and superior antioxidant activity compared to free CuO NPs and algal extract, indicating their potential for oxidative stress modulation. These findings highlight the synergistic effect of bioactive nanoparticles and biodegradable polymers, offering a sustainable and multifunctional platform for biomedical applications, particularly in tissue engineering and wound healing. Overall, this work provides a promising direction for the development of biocompatible, antioxidant-rich nanoscaffolds through the integration of green nanotechnology and electrospinning techniques.

Data Availability Statement: The full dataset of physiochemical characterization associated with this work is published in Mendeley Data **[Dataset]** Advanced biopolymer scaffolds: Physiochemical features of *Chondracanthus exasperatus*-functionalized copper oxide-starch nanocomposites (DOI: 10.17632/99bn3x4yzb.1). Disclosure: The material characterization data and figures (e.g., UV, SEM, FTIR, XRD, TGA, Zeta Potential and particle sizer) presented here were generated from a common dataset and are being reused across multiple related studies on nanomaterials. All biological analyses and conclusions are original to each manuscript.

Conflicts of Interest: The authors declare no conflicts of interest.

REFERENCES

[1] Surendran N, Chandrasekaran G, Raju MV, Chandrasekaran MK, Ahalliya RM, Palanisamy CP, Kanniappan GV, Arcot R, Alharbi NS, Thiruvengadam M. Anti-inflammatory potential of ethanolic extract of Maranta arundinacea L.: Insights from COX-2 modulation and oxidative stress analysis. South African Journal of Botany. 2026; 195: 142-151.

[2] Pei J, Senthilkumar MV, Hessini K, Subramaniyam S, Sivaramakrishnan R, Kanniappan GV, Jayaraman S, Palanisamy CP. Green fabrication of starch/PVA/CuO nanoscaffolds using marine macroalgae extract for enhanced anti-inflammatory activity. Sustainable Chemistry and Pharmacy. 2026; 51: 102397.

[3] Balasubramanian V, Loganathan L, Muthuswamy K, Viswanathan TM, Raju MV, Chandrasekaran MK, Ahalliya RM, Poorasamy J, Palanisamy CP, Dominic S, Kanniappan GV. Anticancer therapeutic efficacy of PEGylated β-galactosidase from Aspergillus terreus in DMBA-induced breast cancer: Toxicological, molecular and histopathological evaluation in Wistar rats. International Journal of Biological Macromolecules. 2026; 360: 151856.

[4] Jayaraman S, Eswaran A, Rajagopal P, Palanisamy CP, Veerakumar P, Veeraraghavan VP, Sirasanagandla SR. Neuroendocrine-associated epigenetic factors in cellular senescence: mechanisms and therapeutic implications. Biogerontology. 2026; 27(2): 64.
[5] Ponnusamy B, Rajagopal P, Palanisamy CP, Veeraraghavan VP, Jayaraman S. Mechanistic Exploration of the anticancer activity of Justicia adhatoda Plant Leaf Ethanolic Extract against Colon Cancer Cells: An in silico and in vitro Approach. Asian Pacific Journal of Cancer Prevention. 2026; 27(3): 1069-1080.
[6] Pei J, Saran VS, Sivaramakrishnan R, Kanniappan GV, Pandurangan V, Jayaraman S, Dhayalan VK, Mironescu M, Mironescu ID, Palanisamy CP. Ultrasonic-assisted, Sargassum ilicifolium (brown marine macroalgae)-mediated biogenic synthesis of CuO nanoparticles incorporated in starch/PVA electrospun nanoscaffolds: In vitro safety and antioxidant efficacy assessment. Bioorganic Chemistry. 2026; 173: 109679.
[7] Raj MAPA, Subramaniyam S, Kanniappan GV, Jayaraman S, Palanisamy CP. Sustainable fabrication of starch/PVA/CuO electrospun nanoscaffolds from Turbinaria ornata (marine macroalgae) extract: Physicochemical characterization and antidiabetic evaluation. Kuwait Journal of Science. 2026; 53(2): 100545.
[8] Pei J, Ganesh NS, Subramaniyam S, Sivaramakrishnan R, Kanniappan GV, Jayaraman S, Palanisamy CP. Sustainable fabrication of starch/PVA/CuO electrospun nanoscaffolds from Padina tetrastromatica (Brown macroalgae) extract: Physicochemical characterization and antidiabetic assessment. Sustainable Chemistry One World. 2026; 9: 100195.
[9] Sakthiraj A, Sivaramakrishnan R, Subramaniyam S, Kanniappan GV, Pandurangan V, Jayaraman S, Dhayalan VK, Mironescu M, Mironescu ID, Palanisamy CP. Starch/PVA electrospun nanoscaffolds loaded with ultrasonic-assisted green-synthesis of CuO nanoparticles from marine macroalgae (Gracilaria corticata) extract: Cytotoxicity and antioxidant analysis. Chemical Physics Impact. 2026; 12: 101018.
[10] Raju M, Chandrasekaran MK, Loganathan L, Ahalliya RM, Mironescu M, Mironescu ID, Palanisamy CP, Kanniappan GV. Lipid remodeling and ferroptosis in phosphatidylcholine-mediated tumor–stroma crosstalk. Frontiers in Molecular Biosciences. 2026; 13: 1742305.
[11] Kunamalla R, Panagal M, Palanisamy CP. Biogenic synthesis and fabrication of starch/PVA/CuO electrospun nanoscaffolds from Sargassum ilicifolium (brown marine macroalgae) extract for anticancer activity on HT-29 and MCF-7 cancer cells. Biocatalysis and Agricultural Biotechnology. 2026; 72: 103923.
[12] Pei J, Govindaraj H, Sivaramakrishnan R, Kanniappan GV, Pandurangan V, Dhayalan VK, Mironescu M, Mironescu ID, Jayaraman S, Palanisamy PC. Sustainable fabrication of biopolymer-based (starch/PVA) nanoscaffolds loaded with green-synthesized CuO nanoparticles from Sargassum wightii (marine macroalgae): Cytocompatibility and antioxidant activity. Biomaterials Advances. 2026; 182: 214660.
[13] Pei J, Perumal NC, Meng P, Long Q, Palanisamy CP. Extracellular vesicle-based biosensors for Alzheimer's disease: A new frontier in precision diagnostics. Ageing Research Reviews. 2026; 113: 102904.
[14] Shree P, Sivaramakrishnan R, Kanniappan GV, Pandurangan V, Jayaraman S, Dhayalan VK, Mironescu M, Mironescu ID, Palanisamy CP. Antioxidant and biocompatible CuO-starch/PVA nanoscaffolds via ultrasonic green synthesis using Turbinaria conoides (brown marine macroalgae). Medicine in Drug Discovery. 2025; 28: 100238.
[15] Gong J, Lin J, Guan T, Pei J, Palanisamy CP, El-AtyFrom AMA. selenium tolerance to nanoplastic antagonism: Comprehensive characterization of L. casei SNUT1 and its extracellular vesicle–nanoselenium complex. Food Bioscience. 2025; 74: 107749.
[16] Poochi SP, Sundarraj R, Raju MV, Chandrasekaran MK, Ahalliya RM, Palanisamy CP, Kanniappan GV, Kondapavuluri BK, Thiruvengadam M. Harnessing Nature: Computational and Experimental Insights Into *Ipomoea obscura* Metabolites for Bladder Cancer Therapy. Chemistry and Biodiversity. 2025; 0: e00909.
[17] Dugganaboyana GK, Kannankumar MKG, Shivaramakrishna S, Raju MV, Chandrasekaran MK, Ahalliya RM, Panneerselvam N, Palanisamy CP, Kanniappan GV. Phytochemical insights, antioxidant activity and therapeutic potential of Cassia senna against prostate cancer in Wistar albino rats. Discover Applied Sciences. 2025; 7:1206.
[18] Natarajan SR, Krishnamoorthy R, Alshuniaber MA, Gatasheh MK, Rajagopal P, Veeraraghavan VP, Palanisamy CP, Jayaraman S. KDM1A Facilitates Oncogenic Potential in Colorectal Cancer Progression Through the Activation of AXIN/GSK3β/β-Catenin Signaling Pathways: Evidence From Integrated Transcriptomics and In Vitro Studies. The Journal of Gene Medicine. 2025; 27(11): e70053.
[19] Guan T, Gong J, Lin J, Palanisamy CP, Jinjin Pei J, El-Aty AMA. Machine learning-driven multimodal optimization of selenium biotransformation and flavor profiling in fermented apple–Yacon functional beverages. Innovative Food Science & Emerging Technologies. 2025; 105: 104198.
[20] Natarajan SR, Krishnamoorthy R, Alshuniaber MA, Alsulami TS, Gatasheh MK, Rajagopal P, Palanisamy CP, Govindan R, Veeraraghavan VP, Jayaraman S. ABCE1 facilitates tumour progression via aerobic glycolysis and inhibits cell death in human colorectal cancer cells through the p53 signalling

pathway. Scientific Reports. 2025; 15: 24674.
[21] Huang Y, Guo H, Liu Y, Jin W, Palanisamy CP, Pei J, Oz F, El-Aty AMA. Effects of Natural Polysaccharides on the Gut Microbiota Related to Human Metabolic Health. Molecular Nutrition & Food Research. 2025; 69:e202400792.
[22] Poornima K, Meenakshi K.C, Manikandan V.R, Shankari G, Prabhu D, Rathi M.A, Palanisamy CP, Balaji R, Gopalakrishnan V.K. Exploring the anticancer potential of Jerantinine A from *Tabernaemontana coronaria* against prostate, breast, and ovarian cancers: A computational approach. *Journal of Complementary and Integrative Medicine*, 2025 22(2): 363–372.
[23] Palanisamy CP, Poompradub S, Sansanaphongpricha K, Jayaraman S, Subramani K. Faridah Sonsudin gGreen synthesis of Nigella sativa-mediated silver nanoparticles for enhanced antibacterial activity and wound healing: Mechanistic insights and biomedical applications. Environmental Nanotechnology, Monitoring & Management. 2025; 24: 101085.
[24] Surendran N, Raju MV, Chandrasekaran MK, Ahalliya RM, Palanisamy CP, Chandrasekaran G, Kanniappan GV. Physicochemical characterization of starch from Maranta arundinacea L.(arrowroot) rhizomes and its inhibition of COX-2: In vivo validation. Bioactive Carbohydrates and Dietary Fibre. 2025; 33: 100465.
[25] Kannappan P, Chandrasekaran MK, Raju MV, Gopalakrishnan S, Dhamodharan P, Ahalliya RM, Palanisamy CP, Raju B, Kanniappan GV. Exploring the anticancer potential of Jerantinine A from Tabernaemontana coronaria against prostate, breast, and ovarian cancers: a computational approach. Journal of Complementary and Integrative Medicine. 2025; 22(02): 363-372.
[26] Pei J, Kumarasamy RV, Jayaraman S, Kanniappan GV, Long Q, Palanisamy CP. Quercetin-functionalized nanomaterials: Innovative therapeutic avenues for Alzheimer's disease management. Ageing Research Reviews. 2025; 104: 102665.
[27] Jayaraman S, Prasad M, Natarajan SR, Krishnamoorthy R, Alshuniaber MA, Gatasheh MK, Veeraraghavan VP, Rajagopal P, Palanisamy CP. Molecular mechanisms underlying the effects of beta-sitosterol on TGF-β1/Nrf2/SIRT1/p53-mediated signaling in the kidney of a high-fat diet and sucrose-induced type-2 diabetic rat. Chemico-Biological Interactions. 2025; 411: 111443.
[28] Huang Y, Guo H, Liu Y, Jin W, Palanisamy CP, Pei J, Oz F, El-Aty AMA. Effects of Natural Polysaccharides on the Gut Microbiota Related to Human Metabolic Health. Molecular Nutrition & Food Research. 2025; e202400792.
[29] Prabhakaran P, Palanisamy CP, Shanmugam A, Damodharan P, Swaminathan H, Devaraj D, Ahalliya RM, Kanniappan GV. Isolation, structural characterization, and molecular docking studies on the bioactive compound from n-Hexane extract of Emilia sonchifolia (L.) DC against the pancreatic cancer target Aurora 2 Kinase. Journal of Complementary and Integrative Medicine. 2024; 22(1): 0290.
[30] Jiang H, Kumarasamy RV, Pei J, Raju K, Kanniappan GV, Palanisamy CP. Integrating engineered nanomaterials with extracellular vesicles: Advancing targeted drug delivery and biomedical applications. Frontiers in Nanotechnology. 2024; 6: 1513683.
[31] Guo H, Liu Y, Wan T, Song D, Palanisamy CP, Geng J, Pei J, Özmen S, El-Aty AMA. Toward personalized cancer management: Role of precision nutrition–diet interventions. Journal of Functional Foods. 2024; 123: 106584.
[32] Natarajan SR, Krishnamoorthy R, Alshuniaber MA, Al-Anazi KM, Farah MA, Rajagopal P, Palanisamy CP, Veeraraghavan VP, Jayaraman S. Identification of FOXM1 as a novel protein biomarker and therapeutic target for colorectal cancer progression: Evidence from immune infiltration and bioinformatic analyses. International Journal of Biological Macromolecules. 282 (Part 4): 137201.
[33] Natarajan PM, Swamikannu B, Sivaraman NM, Stylin AGSQ. Prevention of Oral Cancer: A Comprehensive Guide. Journal of Pharmacy and Bioallied Sciences. 2024; 16(5): S4239-S4241.
[34] Umapathy V, Dhanavel A, Kesavan R, Natarajan PM, Bhuminathan S, Vijayalakshmi P. Anticancer Potential of the Principal Constituent of Piper nigrum, Piperine: A Comprehensive Review. Cureus. 2024; 16(2): e54425.
[35] Umapathy VR, Swamikannu B, Natarajan PM, Devi R, Nandini MS, Vimalarani, Vijayalakshmi P. In Silico Molecular Docking of Ocimum sanctum Phytochemicals: Targeting Key Biomarkers in Oral Cancer. Journal of Pharmacy and Bioallied Sciences. 2024; 16(5): S4792-S4799.
[36] Natarajan PM, Bhuminathan S, Rajan R, Bindu K, Loganathan K, Veerakumar R. The Crucial Role of Smoking Cessation in Preventing Oral Cancer. Journal of Pharmacy and Bioallied Sciences. 2024; 16(5): S4245-S4247.
[37] Swamikannu B, Umapathy VR, Natarajan PM, Nandini MS, Stylin AGSQ, Vimalarani V, Rajinikanth S. Unlocking the Therapeutic Benefits of Artemisia Annua: A Comprehensive Overview of its Medicinal Properties. Journal of Pharmacy and Bioallied Sciences. 2024; 16(5): S4248-S4253.
[38] Natarajan PM. Computational Studies on Recent Congeners of Fluoroquinolones and Nitroimidazoles for Their Use in Periodontal Therapy. Journal of Pharmacy and Bioallied Sciences. 2024; 16(5): S4731-S4740.

[39] Yadalam PK, Arumuganainar D, Natarajan PM, Ardila CM. Artificial intelligence-powered prediction of AIM-2 inflammasome sequences using transformers and graph attention networks in periodontal inflammation. Scientific Reports. 2025; 15: 8733.
[40] Yadalam PK, Chatterjee S, Natarajan PM, Ardila CM. Comparison of light gradient boosting and logistic regression for interactomic hub genes in Porphyromonas gingivalis and Fusobacterium nucleatum-induc ed periodontitis with Alzheimer's disease. Frontiers in Oral Health. 2025; 6:1463458.
[41] Natarajan PM, Bhuminathan S, Leela B, Bindu K, Loganathan K, Ramachandran V. Smoking and its Role in Oral Cancer. Journal of Pharmacy and Bioallied Sciences 16(5): S4242-S4244.
[42] Yadalam PK, Natarajan PM, Ardila CM. Variational graph autoencoder for reconstructed transcriptomic data associated with NLRP3 mediated pyroptosis in periodontitis. Scientific Reports. 2025; 15: 1962.
[43] Daniel Raja FS, Abraham L, Rangasamy K, Saikia K, Rathankumar AK, Mironescu M, Mironescu I, Palanisamy CP, Kanniappan GV. Next-Generation Microbiome Therapeutics: Psychobiotics and Fecal Microbiota Transplants (FMT) for Mental Health Treatment. Frontiers in Cellular and Infection Microbiology. 2026; 16: 1719357.
[44] Dharmaprakash S, Gunasekaran VP, Sivaramakrishnan R, Kanniappan GV, Jayaraman S, Mironescu M, Rajabathar JR, Mironescu ID, Palanisamy CP. Marine macroalgae-mediated ultrasonic-assisted green synthesis of CuO nanoparticles embedded in starch/PVA electrospun nanoscaffolds for in vitro α-amylase and α-glucosidase inhibitory activity. Scientific Reports. 2026.
[45] Natarajan PM, Umapathy VR, Murali A, Swamikannu B. (2022). Computational Simulations of Identified marine-derived Natural Bioactive Compounds As Potential Inhibitors of Oral Cancer. Future Science OA. 2022; 8(3).
[46] Natarajan PM, Umapathy VR. Role of transcriptomics in the study of oral cancer. Frontiers in Oral Health. 2025; 6:1524364.
[47] Vidhyarekha U, Natarajan PM, Bhuminathan S, Sabarinathan J, Suba R, Vijayalakshmi P. Role of artificial intelligence in Oral Cancer. Advances in Public Health. 2024. 2024: 3664408.
[48] Ganesan A, Kumar NG, Natarajan PM, Gauthaman J. Automated classification of elongated styloid processes using deep learning models-an artificial intelligence diagnostics. Frontiers in Oral Health. 2025; 5: 1424840.
[49] Umapathy VR, Natarajan PM, Swamikannu B. Regenerative Strategies in Dentistry: Harnessing Stem Cells, Biomaterials and Bioactive Materials for Tissue Repair. Biomolecules. 2025; 15: 546.
[50] Natarajan PM. Dental Bioinformnatics-Current Scope and Future perspectives. Research Journal of Pharmacy and Technology. 2022;15(5):2351-6.
[51] Ganesan A, Kumar NG, Natarajan PM. Solanum trilobatum leaf extract-derived silver nanoparticles downregulate the PI3K/AKT/mTOR signaling pathway and attenuate oral squamous cell carcinoma cell proliferation. Journal of Herbmed Pharmacology. 2024; 13(2): 300-307.
[52] Perumal MKK, Renuka RR, Subbiah SK, Natarajan PM. Artificial intelligence-driven clinical decision support systems for early detection and precision therapy in oral cancer: a mini review. Frontiers in Oral Health. 2025; 6: 1592428.
[53] Ramesh E, Ganesan A, Lakshmi KC, Natarajan PM. Artificial intelligence-based diagnosis of oral leukoplakia using deep convolutional neural networks Xception and MobileNet-v2. Frontiers in Oral Health. 2025; 6: 1414524.
[54] Ganesan A, Kumar NG, Natarajan PM. Anticancer activity of silver nanoparticles synthesized from aqueous leaf extract of Solanum trilobatum (Purple fruit pea eggplant) on human oral cancer cells. Journal of Herbmed Pharmacololgy. 2024; 13(2): 260-268.
[55] Rajendran MS, Jayaraman S, Khan JM, Jasmine S, Prabhakaran RK, Raju MV, Chandrasekaran MK, Ahalliya RM, Kannappan P, Palanisamy CP, Kanniappan GV. Investigating the colon toxicity and carcinogenic role of monosodium glutamate compared with Dimethylhydrazine in male Wistar rats: Exploring the link to childhood colon cancer risk. Journal of King Saud University - Science. 2024; 36(11): 103507.
[56] Kumarasamy RV, Natarajan P, Umapathy VR, Roy JR, Rab SO, Saeed M, Panagal M, Mironescu M, Srinivasan GP, Palanisamy CP. Clinical Applications and Therapeutic Potentials of Advanced Nanoparticles: A Comprehensive Review on Completed Human Clinical Trials. Frontiers in Nanotechnology. 2024; 6:1479993.
[57] Jin W, Pei JJ, Roy JR, Jayaraman S, Ahalliya RM, Kanniappan GV, Mironescu M, Palanisamy CP. Comprehensive review on single-cell RNA sequencing: A new frontier in Alzheimer's disease research. Ageing Research Reviews. 2024; 274: 102454.
[58] Pei J, Palanisamy CP, Jayaraman S, Natarajan PM, Umapathy VR, Roy JR, Panagal M, Jayaraman S. Curcumin-loaded polymeric nanomaterials as a novel therapeutic strategy for Alzheimer's disease: A comprehensive review. Ageing Research Reviews. 2024; 99: 102393.

[59] Pei J, Palanisamy CP, Jayaraman S, Natarajan PM, Umapathy VR, Roy JR, Thalamati D, Ahalliya RM, Kanniappan GV, Mironescu M. A comprehensive review on starch-based Sustainable Edible Films Loaded with Bioactive Components for Food Packaging. International Journal of Biological macromolecules. 2024; 274 (Part-1): 133332.
[60] Palanisamy CP, poompradub S, Sansanaphongpricha K, Subramani K, Sonsudin F. Increased expression levels of PDGF and VEGF magnify the wound healing potential facilitated by biogenic synthesis of silver nanoparticles. Nano-Structures & Nano-Objects. 2024; 39: 101236.
[61] Pei J, Palanisamy CP, Jayaraman S, Natarajan PM, Umapathy VR, Roy JR, Thalamati D, Ahalliya RM, Kanniappan GV, Mironescu M. Proteomics Profiling of Extracellular Vesicle for Identification of Potential Biomarkers in Alzheimer's Disease: A Comprehensive Review. Ageing Research Reviews. 2024; 99: 102359.
[62] Xi J, Wang T, Xian P, Liu X, Du M, Yang H, Palanisamy CP, Lin W, Long Q. Proteomic insights uncover enhanced neurotherapeutic potential in conditioned mesenchymal stem cell-derived extracellular vesicles. Extracellular Vesicle. 2024; 3: 100037.
[63] Pei J, Natarajan PM, Umapathy VR, Swamikannu B, Sivaraman NM, Krishnasamy L, Palanisamy CP. Advancements in the synthesis and functionalization of zinc oxide-based nanomaterials for enhanced oral cancer therapy. Molecules. 2024; 29(11): 2706.
[64] Gatasheh MK, Natarajan SR, Krishnamoorthy R, Alsulami TS, Rajagopal P, Palanisamy CP, Veeraraghavan VP, Jayaraman S. Molecular analysis to identify novel potential biomarkers as drug targets in colorectal cancer therapy: an integrated bioinformatics analysis. Molecular and Cellular Oncology. 2024; 11(1): 2326699.
[65] Pei J, Yan Y, Jayaraman S, Rajagopal P, Natarajan PM, Umapathy VR, Gopathy S, Roy JR, Sadagopan CS, Thalamati D, Palanisamy CP, Mironescu M. A review on advancements in the application of starch-based nanomaterials in biomedicine: Precision drug delivery and cancer therapy. International Journal of Biological Macromolecules. 2024; 130746.
[66] Pei JJ, Yan Y, Palanisamy CP, Jayaraman S, Natarajan PM, Umapathy VR, Gopathy S, Roy JR, Sadagopan JC, Thalamati D, Mironescu M. Materials-based drug delivery approaches: Recent advances and future perspectives. Green Processing and Synthesis. 2024; 13: 20230094.
[67] Pei JJ, Deng W, Liu Y, Guo Y, Chen J, Abdu H, Khan MR, Palanisamy CP, El-Aty AM. A Comprehensive Review of Cornus officinalis: Health Benefits, Phytochemistry, and Pharmacological Effects for Functional Drug and Food Development. Frontiers in Nutrition. 2023; 10: 1309963.
[68] Alugoju P, Palanisamy CP, Anthikapalli NVA, Jayaraman S, Prasanskulab A, Chuchawankul S, Dyavaiah M, Tencomnao T. Exploring the anti-aging potential of natural products and plant extracts in budding yeast Saccharomyces cerevisiae: A review. F1000Research. 2023; 12: 1265.
[69] Lavanya M, Krishnamoorthy R, Alshuniaber MA, Manoharadas S, Palanisamy CP, Veeraraghavan VP, Jayaraman S, Rajagopal P, Padmini R. Formulation, characterization and evaluation of gelatin-syringic acid/zinc oxide nanocomposite for its effective anticancer, antioxidant and anti-inflammatory activities. Journal of King Saud University-Science. 2023; 35: 102909.